

Targeting Germinal Matrix Hemorrhage–Induced Overexpression of Sodium-Coupled Bicarbonate Exchanger Reduces Posthemorrhagic Hydrocephalus Formation in Neonatal Rats

Qian Li, MD; Yan Ding, PhD; Paul Krafft, MD; Weifeng Wan, MD; Feng Yan, MD; Guangyong Wu, MD; Yixin Zhang, MD; Qunling Zhan, MD; John H. Zhang, MD, PhD

Background—Germinal matrix hemorrhage (GMH) is a leading cause of mortality and lifelong morbidity in preterm infants. Posthemorrhagic hydrocephalus (PHH) is a common complication of GMH. A sodium-coupled bicarbonate exchanger (NCBE) encoded by solute carrier family 4 member 10 gene is expressed on the choroid plexus basolateral membrane and may play a role in cerebrospinal fluid production and the development of PHH. Following GMH, iron degraded from hemoglobin has been linked to PHH. Choroid plexus epithelial cells also contain iron-responsive element-binding proteins (IRPs), IRP1, and IRP2 that bind to mRNA iron-responsive elements. The present study aims to resolve the following issues: (1) whether the expression of NCBE is regulated by IRPs; (2) whether NCBE regulates the formation of GMH-induced hydrocephalus; and (3) whether inhibition of NCBE reduces PHH development.

Methods and Results—GMH model was established in P7 rat pups by injecting bacterial collagenase into the right ganglionic eminence. Another group received iron trichloride injections instead of collagenase. Deferoxamine was administered intraperitoneally for 3 consecutive days after GMH/iron trichloride. Solute carrier family 4 member 10 small interfering RNA or scrambled small interfering RNA was administered by intracerebroventricular injection 24 hours before GMH and followed with an injection every 7 days over 21 days. NCBE expression increased while IRP2 expression decreased after GMH/iron trichloride. Deferoxamine ameliorated both the GMH-induced and iron trichloride–induced decrease of IRP2 and decreased NCBE expressions. Deferoxamine and solute carrier family 4 member 10 small interfering RNA improved cognitive and motor functions at 21 to 28 days post GMH and reduced cerebrospinal fluid production as well as the degree of hydrocephalus at 28 days after GMH.

Conclusions—Targeting iron-induced overexpression of NCBE may be a translatable therapeutic strategy for the treatment of PHH following GMH. (*J Am Heart Assoc.* 2018;7:e007192. DOI: 10.1161/JAHA.117.007192.)

Key Words: brain • germinal matrix hemorrhage • hemorrhage • iron overload • iron-responsive element-binding protein 2 • neonatal ischemia • slc4a10

Germinal matrix hemorrhage (GMH) develops secondary to the rupture of fragile blood vessels within the subependymal brain tissue. It affects between 12.5% and 22% of infants with birth weights <1500 g.^{1,2} Immature blood vessels in the germinal matrix are deficient in autoregulatory mechanisms and may therefore rupture in response to abnormal

fluctuations of cerebral blood flow, caused by cardiorespiratory instability, among others, in the perinatal period.³ Long-term consequences of GMH include developmental delays, cerebral palsy, and posthemorrhagic hydrocephalus (PHH), which pose a relevant social and economic burden on those affected.^{2,4,5} Approximately 25% of premature infants who have GMH will develop progressive PHH and 40% of those who survive the initial events will require surgery for permanent cerebrospinal fluid (CSF) diversion.² The need for CSF diversion, however, is an independent risk factor for poor neurological outcome following GMH.⁶ Insufficient advancements targeting the development of PHH have been made. Noninvasive treatment strategies that effectively reduce PHH formation after GMH would greatly benefit this patient population.

PHH is believed to be caused by an obstruction within the CSF circulation and/or by an imbalance between CSF formation and absorption.⁷ Impaired CSF absorption may be explained by mechanical and inflammatory destruction of the arachnoid

From the Department of Neurology, The Fifth People's Hospital of Chongqing, Chongqing, China (Q.L., Q.Z.); Departments of Physiology and Pharmacology (Y.D., P.K., W.W., F.Y., G.W., Y.Z., J.H.Z.) and Anesthesiology (J.H.Z.), Loma Linda University School of Medicine, Loma Linda, CA.

Correspondence to: John H. Zhang, MD, PhD, Department of Anesthesiology, Loma Linda University, Loma Linda, CA 92354. E-mail: johnzhang3910@yahoo.com

Received July 18, 2017; accepted November 21, 2017.

© 2018 The Authors. Published on behalf of the American Heart Association, Inc., by Wiley. This is an open access article under the terms of the Creative Commons Attribution-NonCommercial License, which permits use, distribution and reproduction in any medium, provided the original work is properly cited and is not used for commercial purposes.

Clinical Perspective

What Is New?

- This is the first study that related iron overload with a sodium transporter on the choroid plexus epithelial cells.

What Are the Clinical Implications?

- It revealed a potential novel mechanism that leads to cerebrospinal fluid overproduction and hydrocephalus and highlighted the role of sodium-coupled bicarbonate exchanger in cerebrospinal fluid production, which can be a novel therapeutic target for posthemorrhagic hydrocephalus.

granulations; however, the mechanisms of increased CSF production after GMH are not well understood. A sodium-coupled bicarbonate exchanger (NCBE) encoded by the solute carrier family 4 member 10 (*slc4a10*) gene is expressed on the basolateral side of choroid plexus epithelial cells, which is reputed to play a role in CSF production.⁸ Indeed, mice with targeted disruption of the *slc4a10* gene developed cerebroventricular systems of small volume, suggesting a pertinent role of this specific ion transporter in CSF.⁹ The choroid plexus epithelial cells also contain iron-responsive element-binding protein (IRP) 1 and IRP2, which bind to sequences of mRNA known as iron-responsive elements, thereby regulating the translation of iron storage and transport proteins. An important consequence of intraventricular hemorrhage is the release of iron from hemoglobin molecules of lysed erythrocytes, which creates a neurotoxic oxidative environment.¹⁰ High iron concentrations have been shown to reduce the binding affinity of IRP1 to iron-responsive elements and may even cause degradation of IRP2.¹¹ Synthesis of the iron storage protein, ferritin, and the iron transporter protein, transferrin, is greatly dependent on IRPs, and thus may be impaired following GMH.^{12,13}

The present study aims to determine whether GMH-induced or iron trichloride (FeCl_3)-induced iron overload decreases IRP1 and IRP2 expressions and increases NCBE expression for possible roles in CSF production and development of PHH. We hypothesize that iron overload decreases IRP1/IRP2 and increases NCBE expression, while increasing CSF production and PHH. Our results confirm our hypotheses and suggest a noncanonical relationship between decreased IRP1/IRP2 levels and increased NCBE levels. Our findings suggest that combined iron chelation and *slc4a10* knockout may be effective in decreasing CSF production and hydrocephalus formation in patients with GMH.

Materials and Methods

The data, analytic methods, and study materials have been made available to other researchers for purposes of reproducing the results or replicating the procedure. The data that

support the findings of this study are available from the corresponding author upon request. Authors will be responsible for maintaining availability.

GMH Modeling and Treatment

All procedures were in compliance with the National Institutes of Health guidelines for the handling of laboratory animals and approved by the Institutional Animal Care and Use Committee at Loma Linda University.

P7 Sprague-Dawley rat pups (stage of brain development is comparable to an infant at 30–32 weeks of gestation) were implemented in this study. We used stereotactic infusion of 0.3 U of bacterial collagenase into the right ganglionic eminence to induce grade III and IV GMH, as previously described.¹⁴ Briefly, rat pups were anesthetized with 3% isoflurane (in mixed air and oxygen) and placed prone onto a stereotactic head frame. Aseptic techniques were used for all animal surgeries. Following a small longitudinal midline scalp incision, the bregma was identified. A 1-mm burr hole was made 1.6 mm rostral and 1.5 mm right lateral relative to the bregma. A 27-gauge needle was inserted stereotactically through the burr hole 2.7 mm in depth and collagenase was infused. Following that, the needle was left in place for an additional 5 minutes to prevent backflow of collagenase along the needle tract. After removal of the syringe, the burr hole was sealed with bone wax and the incision was closed with sutures. Sham animals were subjected to the same procedure excluding infusion of collagenase. A subgroup of naïve animals received intracerebral injections of FeCl_3 , instead of collagenase.

Deferoxamine (100 mg/kg) or its vehicle (PBS) was injected intraperitoneally every 12 hours, starting 1 hour after GMH induction. *slc4a10* small interfering RNA (siRNA) or scrambled siRNA was injected intracerebroventricularly at the following coordinates relative to the bregma: 1.6 mm (rostral), 1.5 mm (left lateral), and 1.7 mm (in depth). *slc4a10* siRNA was administered 1 day before GMH induction and then every 7 days thereafter for 21 consecutive days (for the long-term experiments). *slc4a10* siRNA (Applied Biological Materials Inc.) was packaged in lentivirus targeting multiple sequences, including 1598CCACCGAAGGTCGTATAAGTGAATCGAA;1839 TTCCCTGTCTGCTATACCCGGTTCA;2623GCAGCCACTGT CCTCTCCATCACTCATGT;3060 GTTGATGGACTTCTGTTTACCA AACGGG.

Experiment 1

To determine the time course of IRP2 and NCBE expressions following GMH, animals subjected to GMH were euthanized on days 1, 3, 5, or 7 after surgery and brain tissues were collected for Western blotting and real-time polymerase chain

reaction (PCR). A sham group was included for comparison (n=6 for each group per time point).

Experiment 2

We tested the effects of iron toxicity on IRP1, IRP2, and NCBE expression levels at 3 days after GMH as well as the long-term effects of iron toxicity on neurological deficits at 21 to 28 days after GMH, the rate of CSF production, and the extent of PHH at 28 days after GMH. We administered deferoxamine to chelate iron after GMH/FeCl₃. The following experimental groups were used: sham, GMH+vehicle, GMH+deferoxamine, FeCl₃+vehicle, and FeCl₃+deferoxamine. On day 3 after GMH, a subgroup of animals was euthanized for Western blotting, real-time PCR (n=6 for each group), and immunofluorescence staining (n=4 for sham, GMH+vehicle, GMH+deferoxamine group). All other animals (n=6 for sham, GMH+vehicle, GMH+deferoxamine group), as well as sham+deferoxamine, were included in the long-term experiments to evaluate neurological deficits at 21 to 28 days after GMH. Sham, GMH+vehicle, and GMH+deferoxamine animals were also used to measure the rate of CSF production, as well as the extent of PHH at 28 days after GMH.

Experiment 3

To determine whether knockdown of *slc4a10* ameliorates CSF overproduction and hydrocephalus formation, thereby improving long-term neurological deficits after GMH, the following experimental groups were selected: sham, GMH, GMH+scrambled siRNA, and GMH+*slc4a10* siRNA. On day 3 after GMH, a subgroup of animals was euthanized for Western blotting, real-time PCR (n=6 for each group), and immunofluorescence staining (n=4 for sham, GMH+scrambled siRNA, GMH+*slc4a10* siRNA group). All other animals (n=6 for each group), as well as sham+*slc4a10* siRNA, were included in the long-term experiments to evaluate neurological deficits at 21 to 28 days after GMH. Sham, GMH+scrambled siRNA, and GMH+*slc4a10* siRNA groups were used to measure the rate of CSF production, as well as the extent of PHH at 28 days after GMH.

Preparation of Brain Tissue

At 3 and 28 days after GMH induction, deeply anesthetized (5% isoflurane) animals were subjected to transcatheter perfusion with ice-cold PBS for Western blotting, real-time PCR, or ice-cold PBS followed by 10% formalin for immunohistochemistry and other histological evaluation. Brains were snap-frozen in liquid nitrogen and stored at -80°C (for Western blotting and real-time PCR) or post-fixed in 10% formalin overnight then dehydrated with a sucrose solution

(30%) for an additional 3 days at 4°C (for histology studies). Forebrain samples used for staining were then embedded in optimal cutting temperature compound and stored at -20°C.

Protein Extraction and Western Blotting

Forebrain samples were homogenized in RIPA lysis buffer (Santa Cruz Biotechnology) and supernatants from the homogenates were collected after centrifugation at 20817 g, at 4°C for 30 minutes. The protein concentration was determined using a detergent compatibility assay (Bio-Rad). Thirty micrograms of protein per sample were loaded, run for 30 minutes at 80 V, then 60 minutes at 120 V, followed by protein transfer onto nitrocellulose membranes at 0.45 mm for 120 minutes (Bio-Rad). Membranes were incubated for 2 hours in 5% nonfat milk in Tris-buffered saline containing 0.1% Tween 20. The following primary antibodies were incubated overnight at 4°C: anti-IRP1 and anti-IRP2 (1:1000; Abcam), anti-NCBE (1:500; Origene) and anti-β-Actin (1:1000; Santa Cruz Biotechnology). The membranes were washed and then incubated with the appropriate secondary antibodies (1:4000, Santa Cruz Biotechnology) for 1 hour at room temperature. Enhanced chemiluminescent solution (GE Healthcare and Life Science) was then applied to the membranes and the protein bands were exposed onto radiography films. ImageJ software (4.0, Media Cybernetics) was used to analyze the relative density of the resultant protein immunoblots.

RNA Extraction and Real-Time PCR

RNA was extracted from forebrain homogenates using the Quick-RNA MiniPrep kit (Genesee Scientific) according to the manufacturer's instructions. RNA concentrations were determined by photometric measurement via the NanoDrop 2000 spectrophotometer (PiqLab Biotechnologie GmbH). First-strand cDNA Synthesis Kit (ThermoFisher) was used for reverse transcription. Three micrograms of RNA was reverse transcribed per the manufacturer's instructions. Quantitative real-time PCR was performed on a CFX96 Touch Real-Time PCR Detection System machine using iTaq Universal SYBR Green Supermix (Bio-Rad) according to the manufacturer's instructions. Primers used in the study were as follows: *slc4a10* forward primer 5'-GCA AGG TGC TTT TTC CAG AGG-3', reverse primer 5'-GCT CTT TCT TCC ACC AAG CG-3', IRP1 forward primer 5'-GAC CCA ATG AGG TAC CA GGC-3', reverse primer 5'-TGC TCA TCT TGC TAG CAC CC-3', IRP2 forward primer 5'-ACT CCC CAA GTG CAG GAT AC-3', and reverse primer 5'-CAG CTT CCA ATA GGA CCC GT-3'. GAPDH was used as internal control. The primers were GAPDH forward 5'-CTT CAT TGA CCT CAA CTA CAT G-3' and reverse

5'-GAC TGT GCC GTT GAA CTT GC-3'. The PCR amplification phase consists of 40 cycles of amplification using a plateau of 95°C for 30 seconds for denaturation, followed by a plateau of 60°C for 1 minute for annealing, and a plateau of 72°C for 30 seconds for amplification. All real-time PCRs were performed in triplicates. Results were quantitated using $\Delta\Delta C_t$ method.

Immunohistochemistry and Volumetric Analysis

Following postfixation of the brain samples in formalin, 10- μ m thick coronal sections were cut using a cryostat (Leica Microsystems LM3050S). Brain sections revealing choroid plexus were used for immunohistochemical staining as previously described.¹⁵ Briefly, these brain sections were incubated overnight at 4°C with the following primary antibodies: anti-IRP1 (1:200, Abcam), anti-IRP2 (1:100, Abcam), anti-NCBE (1:50, Origene), and antitransferrin (1:50, Abcam). Sections were then washed and incubated with the appropriate secondary antibodies (1:100, Jackson ImmunoResearch Labs) for 2 hours at room temperature. The tissue slides were then stained with 4',6-diamidino-2-phenylindole (Vector Laboratories), fixed in paramount, and visualized using a fluorescence microscope (Olympus BX51, Olympus Corporation). For histological, volumetric analysis, 16- μ m thick coronal brain sections were cut at 2.5 mm, 1.2 mm, 0.7 mm rostral, and 2.9 mm caudal of the bregma. These brain slices were stained with Nissl and morphometrically analyzed using ImageJ 4.0 (Media Cybernetics) assisted delineation of brain structures, as previously described.¹⁶ The ventricle volume was calculated as average ventricular areas on each slide multiplied by the depth of the cerebroventricular system.

Neurobehavioral Assessment

Morris water maze and rotarod tests were performed in a blinded manner to evaluate cognitive and sensorimotor deficits in rats between 21 and 28 days after GMH induction, as previously described.^{17,18} Briefly, for the water maze test, rats were placed in a round pool (110 cm in diameter) filled with water and trained to find a visible platform (11 cm in diameter). After these cued trials, the platform was slightly submerged and the rats were allowed to find the location of the platform on 10 trials per day for 4 consecutive days. Additionally, at the end of each test day, the platform was removed from the pool (Probe trial). An overhead camera with a computerized tracking system (Noldus Ethovision) recorded the swim path and measured the swim distance and time spent within the probe quadrant. Briefly, for the rotarod test, rats were placed onto a rotarod (Columbus Instruments), consisting of a rotating horizontal cylinder (7 cm in diameter).

Rats had to move along with the rotating cylinder to avoid falling. Rotarod testing started at either 5 or 10 RPM with an acceleration of 2 RPM every 5 seconds. A photobeam circuit detected the fall off the cylinder and the latency to this event was recorded for each animal.

Measuring CSF Production

CSF production was measured by the ventriculo-cisternal perfusion method.¹⁹ Briefly, after introduction of the micropipette in the contralateral lateral ventricle to the GMH site, a second micropipette held in a horizontal position was inserted into the cisterna magna micropipette. After observing CSF in the cisterna magna micropipette, the perfusion was started. The lateral ventricle was perfused with artificial CSF containing 10 mg/mL of fluorescein isothiocyanate dextran (500 000 MW, ThermoFisher) with a total volume of 100 and 80 μ L fluid in the cisterna magna was collected. This procedure lasted for 40 minutes. Sham-operated animals also received the same infusion and withdrawal of fluid. The rate of CSF production was calculated from the equation $V_f = r_i (C_i - C_o) / C_o$. V_f was the CSF production rate (μ L/min), r_i was the infusion rate (1 μ L/min), C_i was the dextran concentration of inflow solution (10 mg/mL), and C_o was the dextran concentration of outflow solution. Absorbance of the fluid collected was measured at 498 nm. Concentrations of the solution were calculated based on a standard curve.

Statistical Analysis

Statistical analysis was performed using Sigma Plot10.0 and Sigma Stat3.5 (Systat Software). Data were presented as mean \pm SEM and evaluated by 1-way ANOVA followed by Tukey or Student–Newman–Keuls tests. P values <0.05 were considered statistically significant.

Results

GMH Decreased IRP2 Expression and Increased NCBE Expression

A time-course study was conducted to determine IRP2 and NCBE protein expression and gene transcription in the forebrain of rats on 1, 3, 5, and 7 days following GMH induction. We found that IRP2 protein expression was significantly decreased in GMH animals starting from day 1 to day 5 compared with the sham group or GMH animals euthanized on day 7 after surgery ($P < 0.05$; Figure 1A). IRP2 protein expression was found to be similar on day 7 after GMH compared with the sham group ($P > 0.05$). Reversely, the expression of the NCBE was found to be significantly elevated

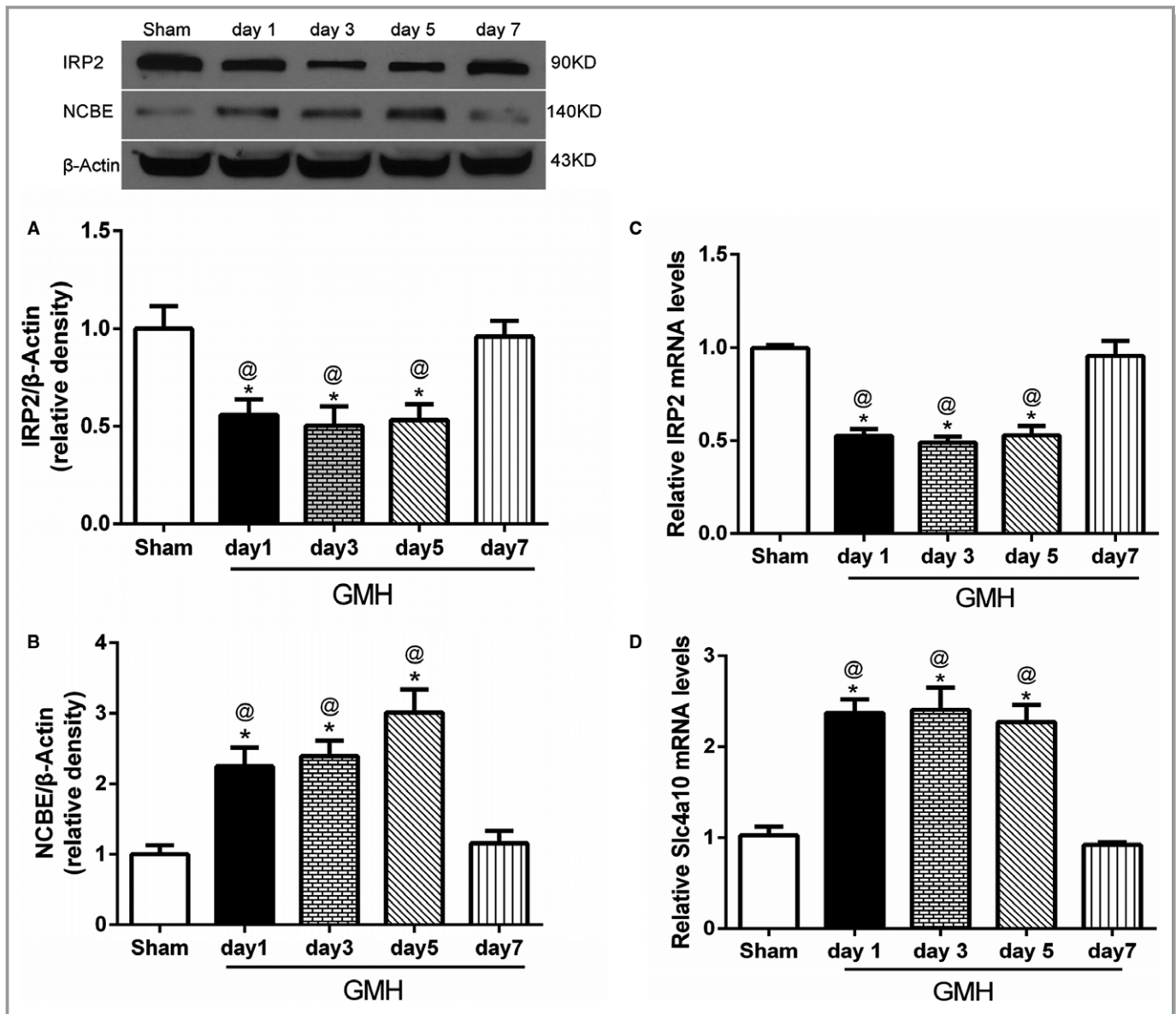


Figure 1. Germinal matrix hemorrhage (GMH) decreased indicates iron-responsive element-binding protein 2 (IRP2) expression and increased sodium-coupled bicarbonate exchanger (NCBE) expression following GMH. A and B, Representative image of Western blot and quantitative of NCBE and IRP2 in rat brain after different time of GMH. C and D, Quantification of the relative mRNA levels of solute carrier family 4 member 10 (slc4a10) and IRP2. N=6 per group. Data are expressed as mean \pm SEM. One-way ANOVA followed by Tukey test. * P <0.05 vs sham. @ P <0.05 vs day 7.

following GMH between day 1 and day 5 compared with the sham or GMH day 7 group (P <0.05; Figure 1B) but was found to be similar to sham on day 7 after GMH (P >0.05). IRP2 and slc4a10 mRNA levels were also measured in the tissue samples collected on 1, 3, 5, and 7 days following GMH induction. The real-time PCR data revealed that IRP2 mRNA levels were significantly decreased while slc4a10 mRNA levels were significantly elevated on days 1, 3, and 5 after GMH compared with sham or the GMH day 7 group (P <0.05; Figure 1C and 1D). IRP2 expression as well as gene

transcription was negatively associated with NCBE expression and slc4a10 gene transcription following GMH.

Iron Toxicity Increased Expression of NCBE After GMH/ FeCl_3

The protein expression of NCBE as well as slc4a10 gene transcription was measured on day 3 after surgery in the following groups: sham, GMH+vehicle, FeCl_3 +vehicle, GMH+deferoxamine, and FeCl_3 +deferoxamine. Interestingly,

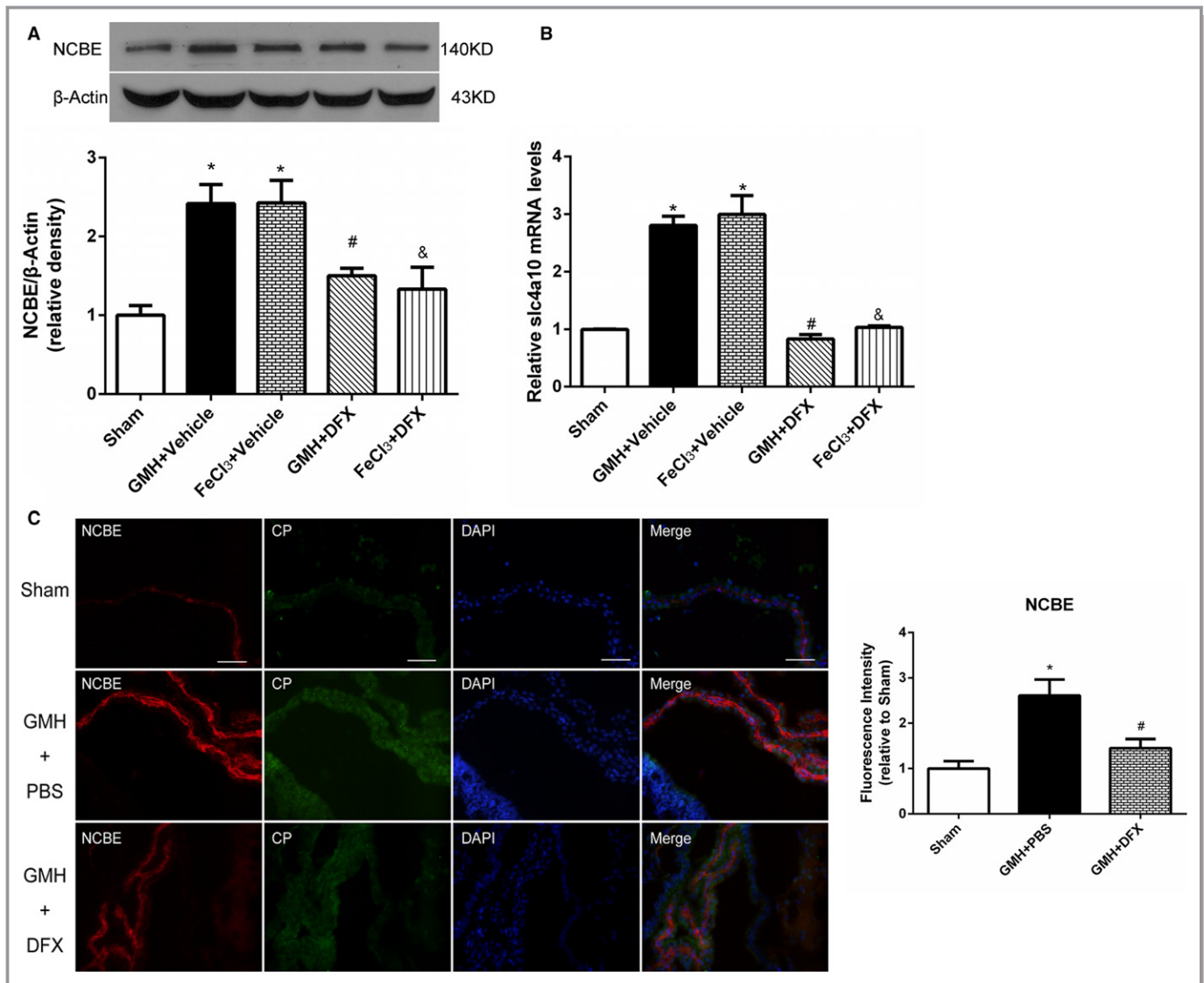


Figure 2. Upregulation of sodium-coupled bicarbonate exchanger (NCBE) induced by germinal matrix hemorrhage (GMH)/iron trichloride (FeCl₃) was related to iron. A, Representative image of Western blot and quantitative of NCBE in rat brain treated by deferoxamine (DFX) after GMH or FeCl₃. B, Quantification of the relative mRNA levels of solute carrier family 4 member 10 (slc4a10). C, Representative immunostaining images of NCBE on choroid plexus (CP) basolateral membrane. Scale bars, 100 μm. N=4 to 6 per group. Data are expressed as mean±SEM. One-way ANOVA followed by Tukey test. * $P<0.05$ vs sham; # $P<0.05$ vs GMH+vehicle; & $P<0.05$ vs FeCl₃+vehicle. DAPI indicates 4',6-diamidino-2-phenylindole.

GMH as well as FeCl₃ administration resulted in a significant increase in both protein and mRNA level of NCBE/slca10 ($P<0.05$; Figure 2A and 2B) compared with the sham group. The iron chelator deferoxamine significantly decreased the protein expression of NCBE after GMH ($P<0.05$ versus GMH+vehicle; Figure 2A) as well as after FeCl₃ administration ($P<0.05$ compared with FeCl₃+vehicle). Similarly, deferoxamine decreased the mRNA level of slca10 after GMH ($P<0.05$; Figure 2B) and FeCl₃ administration ($P<0.05$) compared with the respective vehicle group. The expression of NCBE in the choroid plexus was evaluated via immunohistochemical staining of forebrain at 3 days after surgery. The following

groups were compared: sham, GMH+vehicle, and GMH+deferoxamine. As expected, NCBE localized basolateral membrane in choroid plexus cells (Figure 2C). Representative microphotographs demonstrated seemingly increased expression of NCBE after GMH administration (GMH+vehicle), which was reduced after deferoxamine treatment.

Deferoxamine Restored GMH/FeCl₃ Reduced IRP2 Expression

The protein and mRNA levels of IRP1 and IRP2 were measured on day 3 after surgery in the following groups: sham,

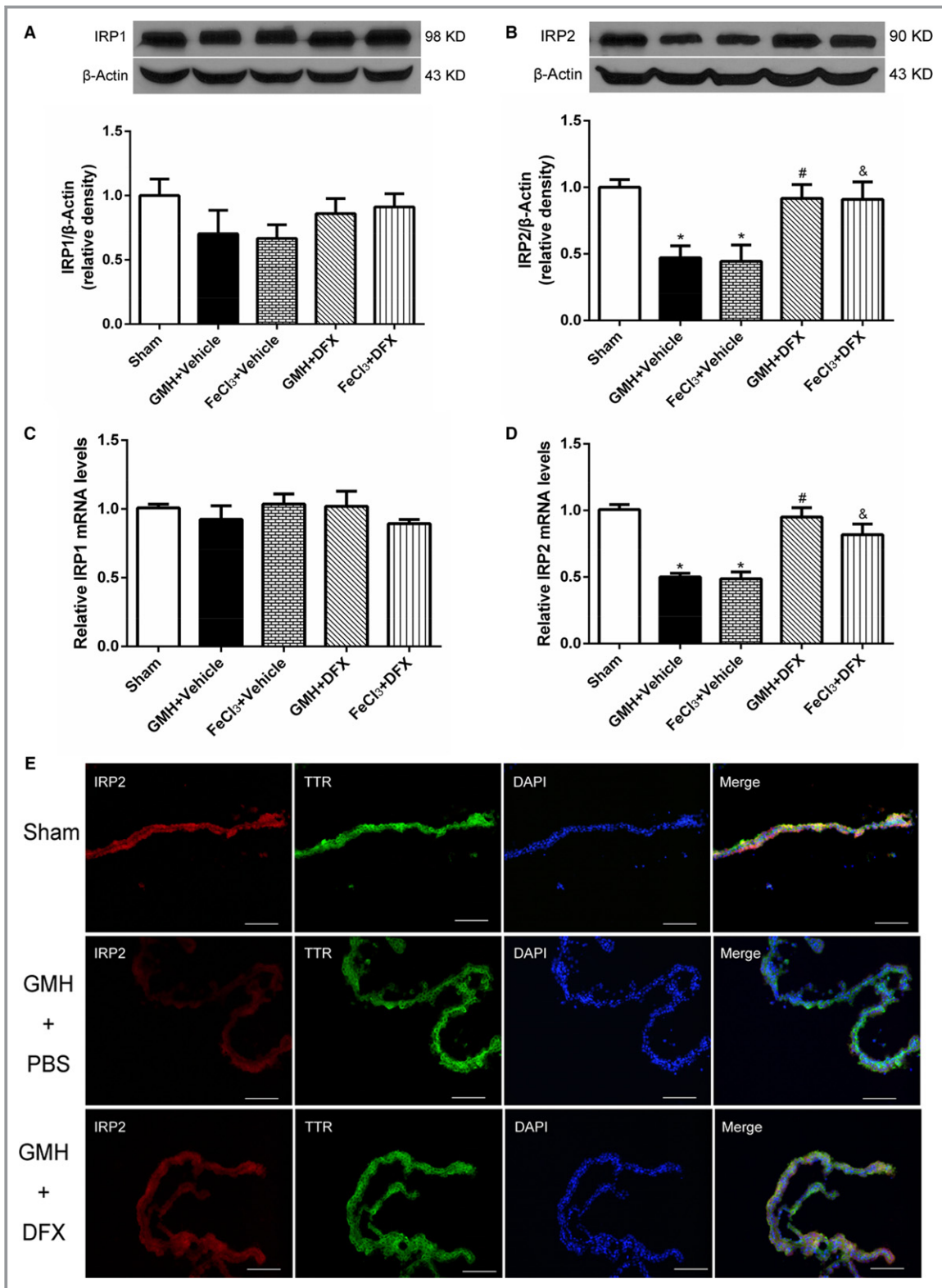


Figure 3. Downregulation of iron-responsive element-binding protein 2 (IRP2) but not IRP1 was related to iron overload after germinal matrix hemorrhage (GMH)/iron trichloride (FeCl₃). A and B, Representative image of Western blot and quantitative of IRP1 and IRP2 in rat brain treated by deferoxamine (DFX) after GMH or FeCl₃. C and D, Quantification of the relative mRNA levels of IRP1 and IRP2. E, Representative immunostaining images of IRP2 on choroid plexus (CP). Scale bars, 100 μ m. N=4 to 6 per group. Data are expressed as mean \pm SEM. One-way ANOVA followed by Tukey test. * P <0.05 vs sham; # P <0.05 vs GMH+vehicle; & P <0.05 vs FeCl₃+vehicle. DAPI indicates 4',6-diamidino-2-phenylindole.

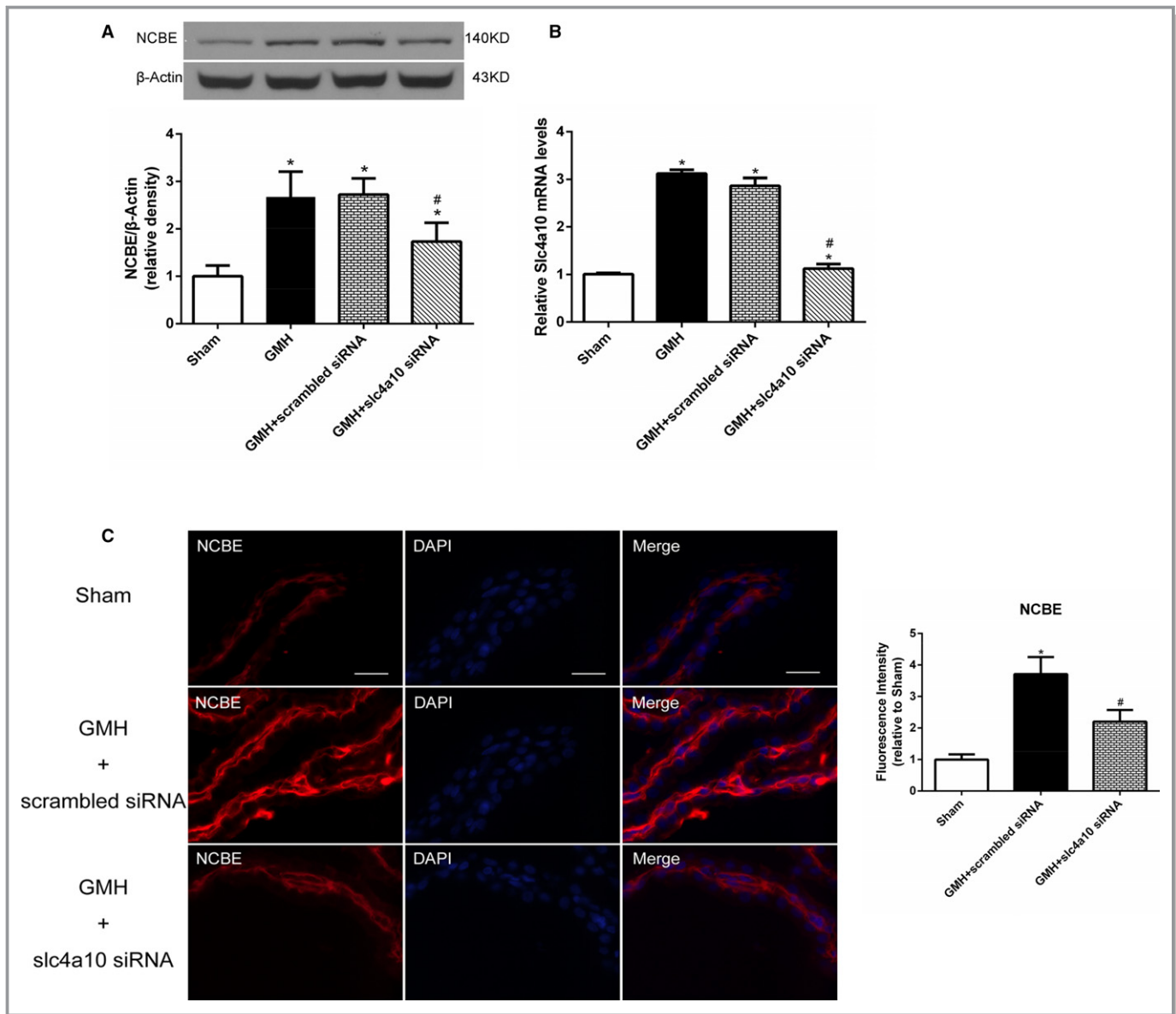


Figure 4. Intracerebroventricular injection of solute carrier family 4 member 10 (slc4a10) small interfering RNA (siRNA) 24 hours before germinal matrix hemorrhage (GMH) decreased sodium-coupled bicarbonate exchanger (NCBE) expression. A, Representative image of Western blot and quantitative of NCBE in rat brain after treated by siRNA. B, Quantification of the relative mRNA levels of slc4a10. C, Representative immunostaining images of NCBE on choroid plexus (CP). N=4 to 6 per group. Data are expressed as mean±SEM. One-way ANOVA followed by Tukey test. * $P<0.05$ vs sham; # $P<0.05$ vs GMH+scrambled siRNA. DAPI indicates 4',6-diamidino-2-phenylindole.

GMH+vehicle, FeCl₃+vehicle, GMH+deferoxamine, and FeCl₃+deferoxamine. No significant changes in IRP1 protein expression nor in IRP1 mRNA were identified between all groups ($P>0.05$; Figure 3A and 3C). The protein expression of IRP2, however, was found to be significantly decreased in the GMH+vehicle and FeCl₃+vehicle group compared with sham ($P<0.05$; Figure 3B). The decrease in IRP2 expression after GMH and FeCl₃ administration was effectively reversed by deferoxamine compared with the respective vehicle groups ($P<0.05$). Similarly, the level of IRP2 mRNA was significantly decreased in the GMH+vehicle and FeCl₃+vehicle group

compared with sham ($P<0.05$; Figure 3D). The decrease in IRP2 mRNA after GMH and FeCl₃ administration was also reversed by deferoxamine, compared with the respective vehicle groups ($P<0.05$). The expression of IRP2 within the choroid plexus was evaluated via immunohistochemical staining of forebrain slides obtained at 3 days after surgery. The following groups were compared: sham, GMH+vehicle, and GMH+deferoxamine. Antitransferrin antibody was used to identify the choroid plexus within the brain. IRP2 and antitransferrin were colocalized within the same cells (Figure 3E). Representative microphotographs demonstrated

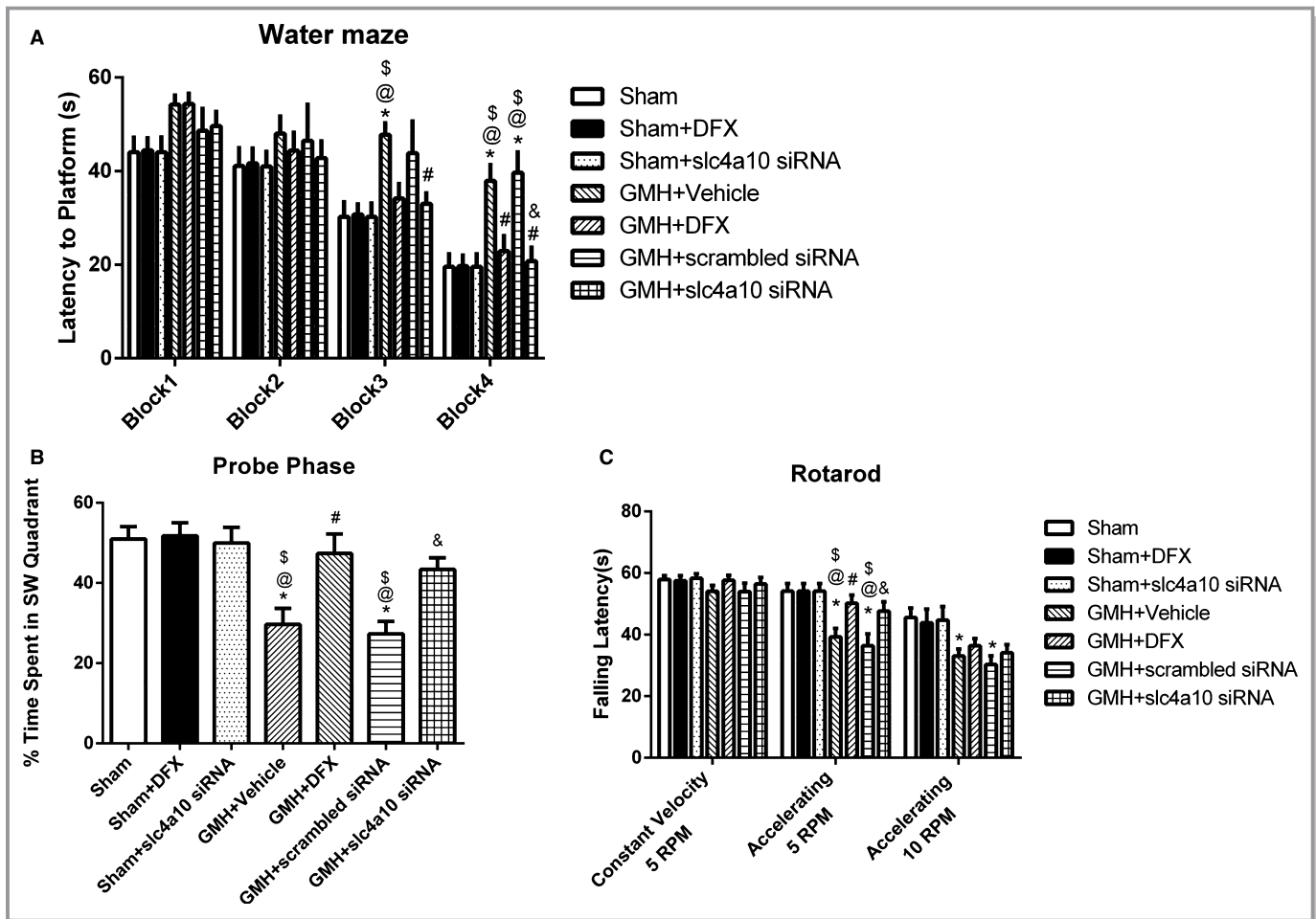


Figure 5. Deferoxamine (DFX) and solute carrier family 4 member 10 (slc4a10) knockdown improved neurological function 21 to 28 days after germinal matrix hemorrhage (GMH). A, Latency to platform of rat after GMH. B, Probe phase data of time rat spent in the southwest (SW) quadrant. C, Rotarod data of the long-term sensorimotor function of rat. N=6 per group. Data are expressed as mean±SEM. One-way ANOVA followed by Tukey test. * $P<0.05$ vs sham; @ $P<0.05$ vs Sham+DFX; \$ $P<0.05$ vs Sham+slc4a10 siRNA; # $P<0.05$ vs GMH+vehicle; & $P<0.05$ vs GMH+scrambled small interfering RNA (siRNA).

seemingly decreased expressions of IRP2 after GMH (GMH+vehicle), which was ameliorated after deferoxamine treatment.

slc4a10 Gene Silencing Decreased NCBE Expression After GMH

The effectiveness of intracerebroventricular injection of slc4a10 siRNA was evaluated. One day before GMH surgery, slc4a10 siRNA or its control was injected into the left lateral ventricle of rat pups. Western blot and real-time PCR were conducted at 3 days after GMH induction to evaluate the effectiveness of slc4a10 knockdown. The protein expression of NCBE was significantly decreased after slc4a10 siRNA injection compared with the vehicle and vehicle+scrambled siRNA groups ($P<0.05$; Figure 4A). Similarly, slc4a10 mRNA was significantly decreased after siRNA injection compared with the vehicle and vehicle+scramble siRNA groups ($P<0.05$;

Figure 4B). The expression of slc4a10 within the choroid plexus was evaluated via immunohistochemical staining of forebrain slides obtained at 3 days after surgery. The following groups were compared: sham, GMH+scrambled siRNA, and GMH+slc4a10 siRNA. NCBE localized basolateral membrane in choroid plexus cells (Figure 4C). Representative microphotographs demonstrated increased expression of NCBE after scramble siRNA injection; however, slc4a10 siRNA effectively reduced NCBE expression within the choroid plexus after GMH induction.

Deferoxamine and slc4a10 Knockdown Improved Neurological Function After GMH

Neurobehavioral deficits were evaluated between day 21 and 28 after GMH. The following groups were compared: sham, sham+deferoxamine, GMH+vehicle, GMH+deferoxamine, sham+slc4a10 siRNA, GMH+scrambled siRNA, and

GMH+slc4a10 siRNA. During the Morris water maze trials, GMH+vehicle animals required significantly longer periods to find the platform compared with sham ($P<0.05$; Figure 5A, block 3). GMH+vehicle and GMH+scramble siRNA animals performed significantly worse than sham animals ($P<0.05$; Figure 5A, block 4). The greater amount of time required by vehicle animals to find the platform during water maze testing was significantly reduced by administration of slc4a10 siRNA in block 3 and by administration of deferoxamine or slc4a10 siRNA in block 4 compared with the respective vehicle groups ($P<0.05$). Furthermore, rodents of the GMH+vehicle and GMH+scrambled siRNA groups spent less time in the correct quadrant during the probe trials compared with either the sham group or animals of the respective vehicle groups ($P<0.05$; Figure 5B), which indicated a significant loss of special memory in GMH animals. The latter was effectively ameliorated by deferoxamine treatment and slc4a10 gene silencing. Similarly, GMH animals (GMH+vehicle and GMH+scramble siRNA) fell faster off the rotating cylinder at a starting speed of 5 RPM compared with the sham, GMH+deferoxamine, and GMH+slc4a10 siRNA groups ($P<0.05$; Figure 5C). GMH animals demonstrated a worse performance than sham animals during rotarod testing at a starting speed of 10 RPM ($P<0.05$); however, no significant improvement was found after deferoxamine treatment or slc4a10 knockdown ($P>0.05$). In general, deferoxamine and slc4a10 siRNA had no effect on sham-operated animals.

Deferoxamine and slc4a10 Gene Silencing Reduced CSF Production After GMH

CSF production was evaluated in sham, GMH+vehicle, GMH+deferoxamine, GMH+scramble siRNA, and GMH+slc4a10 siRNA animals at 28 days after surgery. CSF production rate was found to be significantly increased in untreated GMH animals (GMH+vehicle and GMH+scrambled siRNA) compared with sham animals ($P<0.05$; Figure 6). Deferoxamine treatment and slc4a10 gene silencing resulted in significantly reduced CSF production rates compared with the respective vehicle group ($P<0.05$).

Deferoxamine and slc4a10 Knockdown Ameliorated PHH After GMH

The extent of PHH was evaluated in sham, GMH+vehicle, GMH+deferoxamine, GMH+scrambled siRNA, and GMH+slc4a10 siRNA animals at 28 days after surgery. Representative microphotographs of Nissl-stained coronal brain sections were obtained (Figure 7A). Volumetric analysis of coronal brain slides demonstrated significantly increased volumes of the cerebroventricular system of untreated GMH animals (GMH+vehicle and GMH+scrambled siRNA) compared

with either sham or GMH+deferoxamine and GMH+slc4a10 siRNA animals ($P<0.05$; Figure 7B). GMH+vehicle and GMH+scrambled siRNA animals were also found to have decreased cortical thicknesses compared with the sham group ($P<0.05$; Figure 7C). Deferoxamine treatment and slc4a10 gene silencing tended to ameliorate the loss of cortical thickness after GMH; however, no significant difference was achieved ($P>0.05$). Furthermore, GMH+vehicle and GMH+scrambled siRNA animals demonstrated significant white matter losses compared with the sham group ($P<0.05$; Figure 7D). Deferoxamine treatment and slc4a10 gene silencing tended to ameliorate the white matter loss after GMH; however, no significant difference was achieved ($P>0.05$).

Discussion

The formation of PHH is a well-described and common complication following GMH.² Currently, there is no effective treatment for PHH other than surgical shunting. In fact, the need for CSF diversion via ventriculoperitoneal or ventriculo-pleural shunt placement is an independent risk factor for an adverse neurological outcome following GMH.⁶ While PHH is believed to be caused by an obstruction within the CSF circulation and/or by an imbalance between CSF formation and absorption,⁷ insufficient advancements have been made targeting or preventing its formation. Intracerebroventricular

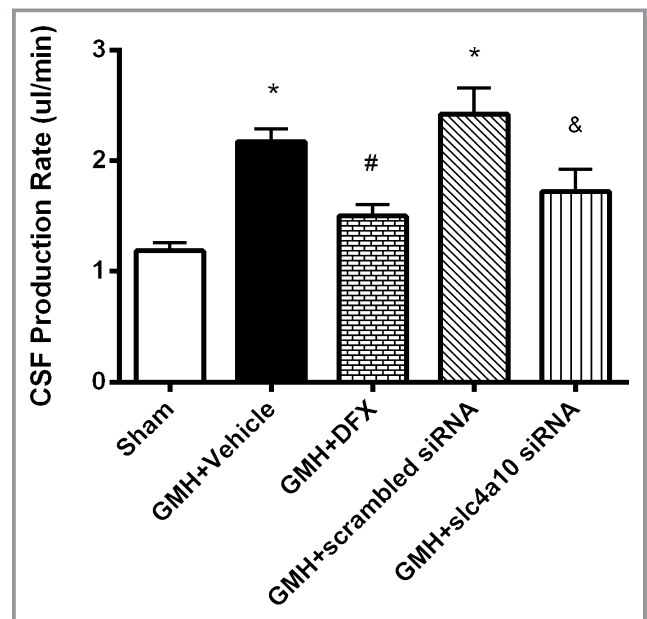


Figure 6. Deferoxamine (DFX) and solute carrier family 4 member 10 (slc4a10) knockdown reduced cerebrospinal fluid (CSF) production 28 days after germinal matrix hemorrhage (GMH). N=6 per group. Data are expressed as mean±SEM. One-way ANOVA followed by Tukey test. * $P<0.05$ vs sham. # $P<0.05$ vs GMH+vehicle. & $P<0.05$ vs GMH+scrambled small interfering RNA (siRNA).

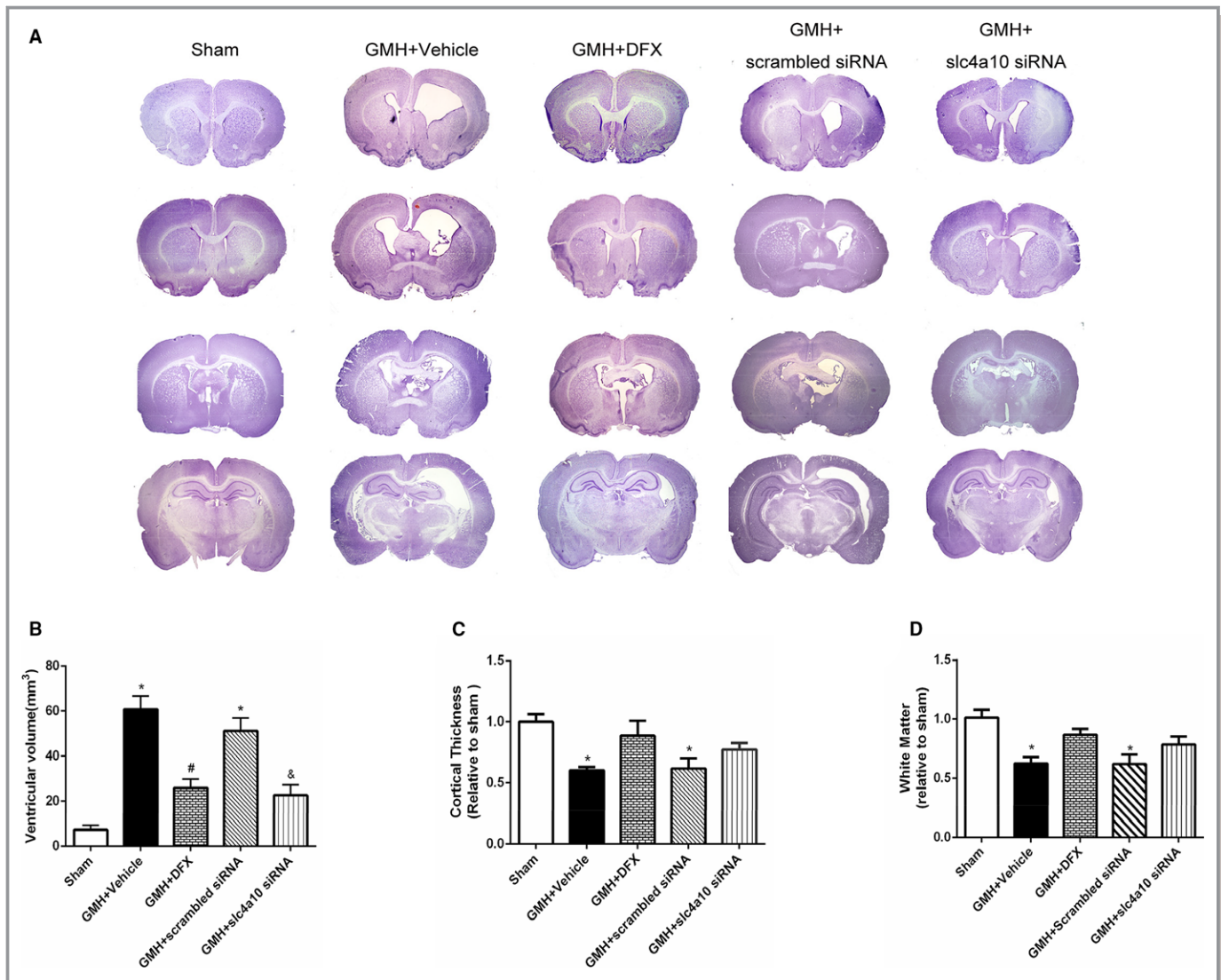


Figure 7. Deferoxamine (DFX) and solute carrier family 4 member 10 (slc4a10) knockdown reduced posthemorrhagic hydrocephalus 28 days after germinal matrix hemorrhage (GMH). Representative microphotographs of Nissl-stained brain sections. (A) Quantification of (B) ventricular volume, (C) cortical thickness, and (D) white matter loss at 28 days after GMH. N=6 per group. Values are expressed as mean±SEM. One-way ANOVA followed by Tukey test. * $P<0.05$ vs sham, # $P<0.05$ vs GMH+vehicle, & $P<0.05$ vs GMH+scrambled small interfering RNA (siRNA).

accumulation of iron, resulting from degraded hemoglobin, has been linked to the development of PHH.¹⁰ Using a preclinical rat pup model of GMH, which has been shown to induce PHH,^{14,18} we attempted to investigate whether GMH-induced iron overload decreases IRP1 and IRP2 expressions, and increases NCBE overexpression, resulting in increased CSF production and consequent PHH formation. We further attempted to evaluate whether iron chelation via deferoxamine or slc4a10 knockdown decreases the rate of CSF production, thereby decreasing hydrocephalus formation and improving neurobehavioral outcomes after GMH.

Our data showed that mRNA and protein levels of slc4a10/NCBE significantly increased on days 1, 3, and 5 after GMH. Furthermore, IRP2 mRNA and protein levels were inversely related to slc4a10/NCBE. Interestingly, IRP1

expression was preserved after GMH. We further demonstrated increased NCBE expression localized on the choroid plexus basolateral membrane, the main source of CSF production. Since NCBE protein is significantly involved in CSF production, under pathophysiological circumstances, overexpression of the transporter could result in increased CSF production, thereby promoting PHH formation following GMH. Indeed, the CSF production rate significantly increased after GMH. Furthermore, iron chelation via deferoxamine and slc4a10 knockdown reduced the CSF production rate, which was associated with decreased ventricular dilation and improved neurobehavioral outcomes. These findings suggest that NCBE upregulation seems to be linked to iron toxicity, since improvements were observed after deferoxamine treatment, and possibly associated with IRP2. However, GMH did

not significantly alter the expression of IRP1. The mechanism still needs to be further identified.

The choroid plexus is an epithelial layer in the ventricles specialized for CSF production.^{20,21} It has relatively high expression of iron transport and iron-dependent metabolic proteins relative to other brain regions.²² IRP1 and IRP2 are sensitive to cellular iron content and mediate changes in iron metabolism by binding to iron response elements on target mRNAs to alter their translation. Specifically, in the setting of iron overloading, IRP1 undergoes conformational changes, whereas IRP2 undergoes proteasomal degradation, both of which decrease IRP activity.¹¹ While IRP1 is more abundant in most cell types, IRP2 is strongly expressed in brain.²³ In red blood cells, at least, lack of IRP2 is not fully compensated by IRP1.²⁴ Following GMH, red blood cells enter the cerebroventricular system and release heme iron, which may adversely alter choroid plexus function. CSF secretion at the choroid plexus involves several ion transporters on both the basolateral and luminal membranes in which ions are pumped into the cerebroventricular system while water follows the osmotic gradient.²⁵ NCBE expressed on the choroid plexus plays an important role in CSF production. *slc4a10* knockout seems to be more deleterious than the knockouts of other transporters implemented in CSF secretion.^{25,26} Indeed, mice with targeted *slc4a10* gene disruption have smaller cerebrovascular systems compared with wild types.⁹ There are multiple ion transporters expressed within the epithelial cells of the choroid plexus, such as sodium bicarbonate cotransporter 1, sodium-proton exchanger protein, and aquaporin 1, contributing to CSF secretion. However, NCBE might play a prominent role in CSF production since it is the only major transporter on the basolateral side of the epithelial cells.^{25–27} While genes of similar ion transporters, such as *slc11a2* and *slc40a1*, are regulated by IRPs through iron responsive elements,^{28,29} no such association between IRPs and NCBE is known.

Study Limitations

One of the limitations of this study is that we mainly focused on how iron overload is associated with NCBE, a major transporter located on the basolateral side. However, aquaporin 1 and Na⁺-K⁺-ATPase, located on the luminal side of the epithelial cells, also play a role in CSF production. Whether GMH causes any functional changes on the luminal side or whether there are any compensatory mechanisms with NCBE knockdown warrants further investigation.

Conclusions

In the present study, we demonstrated that GMH-induced iron overload decreases IRP2 expression, which was associated with an overexpression of NCBE. The latter was, at least in part, likely

responsible for an increase in CSF production and consequent PHH formation. We believe that targeting the cerebroventricular iron and choroid plexus NCBE is a potential treatment strategy to decrease CSF production and hydrocephalus formation may improve neurological outcomes after GMH.

Sources of Funding

This research was supported by National Institutes of Health grant R01 NS078755 to J.H. Zhang.

Disclosures

None.

References

- Hefti MM, Trachtenberg FL, Haynes RL, Hassett C, Volpe JJ, Kinney HC. A century of germinal matrix intraventricular hemorrhage in autopsied premature infants: a historical account. *Pediatr Dev Pathol*. 2016;19:108–114.
- Murphy BP, Inder TE, Rooks V, Taylor GA, Anderson NJ, Mogridge N, Horwood LJ, Volpe JJ. Posthaemorrhagic ventricular dilatation in the premature infant: natural history and predictors of outcome. *Arch Dis Child Fetal Neonatal Ed*. 2002;87:F37–F41.
- Ballabh P. Pathogenesis and prevention of intraventricular hemorrhage. *Clin Perinatol*. 2014;41:47–67.
- Vohr BR, Wright LL, Dusick AM, Mele L, Verter J, Steichen JJ, Simon NP, Wilson DC, Broyles S, Bauer CR, Delaney-Black V, Yolton KA, Fleisher BE, Papile LA, Kaplan MD. Neurodevelopmental and functional outcomes of extremely low birth weight infants in the National Institute of Child Health and Human Development Neonatal Research Network, 1993–1994. *Pediatrics*. 2000;105:1216–1226.
- The Vermont-Oxford Trials Network: very low birth weight outcomes for 1990. Investigators of the Vermont-Oxford Trials Network Database Project. *Pediatrics*. 1993;91:540–545.
- Adams-Chapman I, Hansen NI, Stoll BJ, Higgins R; NICHD Research Network. Neurodevelopmental outcome of extremely low birth weight infants with posthemorrhagic hydrocephalus requiring shunt insertion. *Pediatrics*. 2008;121:e1167–e1177.
- Symms NP, Oi S. Theories of cerebrospinal fluid dynamics and hydrocephalus: historical trend. *J Neurosurg Pediatr*. 2013;11:170–177.
- Damkier HH, Brown PD, Praetorius J. Cerebrospinal fluid secretion by the choroid plexus. *Physiol Rev*. 2013;93:1847–1892.
- Jacobs S, Ruusuvuori E, Sipila ST, Haapanen A, Damkier HH, Kurth I, Hentschke M, Schweizer M, Rudhard Y, Laatikainen LM, Tynnela J, Praetorius J, Voipio J, Hubner CA. Mice with targeted *Slc4a10* gene disruption have small brain ventricles and show reduced neuronal excitability. *Proc Natl Acad Sci USA*. 2008;105:311–316.
- Xiong XY, Wang J, Qian ZM, Yang QW. Iron and intracerebral hemorrhage: from mechanism to translation. *Transl Stroke Res*. 2014;5:429–441.
- Muckenthaler MU, Galy B, Hentze MW. Systemic iron homeostasis and the iron-responsive element/iron-regulatory protein (IRE/IRP) regulatory network. *Annu Rev Nutr*. 2008;28:197–213.
- Casey JL, Koeller DM, Ramin VC, Klausner RD, Harford JB. Iron regulation of transferrin receptor mRNA levels requires iron-responsive elements and a rapid turnover determinant in the 3′ untranslated region of the mRNA. *EMBO J*. 1989;8:3693–3699.
- Hentze MW, Caughman SW, Rouault TA, Barriocanal JG, Dancis A, Harford JB, Klausner RD. Identification of the iron-responsive element for the translational regulation of human ferritin mRNA. *Science*. 1987;238:1570–1573.
- Lekic T, Manaenko A, Rolland W, Krafft PR, Peters R, Hartman RE, Altay O, Tang J, Zhang JH. Rodent neonatal germinal matrix hemorrhage mimics the human brain injury, neurological consequences, and post-hemorrhagic hydrocephalus. *Exp Neurol*. 2012;236:69–78.
- Ostrowski RP, Colohan AR, Zhang JH. Mechanisms of hyperbaric oxygen-induced neuroprotection in a rat model of subarachnoid hemorrhage. *J Cereb Blood Flow Metab*. 2005;25:554–571.

16. Huang B, Krafft PR, Ma Q, Rolland WB, Caner B, Lekic T, Manaenko A, Le M, Tang J, Zhang JH. Fibroblast growth factors preserve blood-brain barrier integrity through RhoA inhibition after intracerebral hemorrhage in mice. *Neurobiol Dis*. 2012;46:204–214.
17. Flores JJ, Klebe D, Rolland WB, Lekic T, Krafft PR, Zhang JH. PPARgamma-induced upregulation of CD36 enhances hematoma resolution and attenuates long-term neurological deficits after germinal matrix hemorrhage in neonatal rats. *Neurobiol Dis*. 2016;87:124–133.
18. Klebe D, Krafft PR, Hoffmann C, Lekic T, Flores JJ, Rolland W, Zhang JH. Acute and delayed deferoxamine treatment attenuates long-term sequelae after germinal matrix hemorrhage in neonatal rats. *Stroke*. 2014;45:2475–2479.
19. Oshio K, Watanabe H, Song Y, Verkman AS, Manley GT. Reduced cerebrospinal fluid production and intracranial pressure in mice lacking choroid plexus water channel Aquaporin-1. *FASEB J*. 2005;19:76–78.
20. Lee JY, Keep RF, He Y, Sagher O, Hua Y, Xi G. Hemoglobin and iron handling in brain after subarachnoid hemorrhage and the effect of deferoxamine on early brain injury. *J Cereb Blood Flow Metab*. 2010;30:1793–1803.
21. Simard PF, Tosun C, Melnichenko L, Ivanova S, Gerzanich V, Simard JM. Inflammation of the choroid plexus and ependymal layer of the ventricle following intraventricular hemorrhage. *Transl Stroke Res*. 2011;2:227–231.
22. Rouault TA, Zhang DL, Jeong SY. Brain iron homeostasis, the choroid plexus, and localization of iron transport proteins. *Metab Brain Dis*. 2009;24:673–684.
23. Henderson BR, Seiser C, Kuhn LC. Characterization of a second RNA-binding protein in rodents with specificity for iron-responsive elements. *J Biol Chem*. 1993;268:27327–27334.
24. Cooperman SS, Meyron-Holtz EG, Olivier-Wilson H, Ghosh MC, McConnell JP, Rouault TA. Microcytic anemia, erythropoietic protoporphyria, and neurodegeneration in mice with targeted deletion of iron-regulatory protein 2. *Blood*. 2005;106:1084–1091.
25. Damkier HH, Praetorius J. Genetic ablation of Slc4a10 alters the expression pattern of transporters involved in solute movement in the mouse choroid plexus. *Am J Physiol Cell Physiol*. 2012;302:C1452–C1459.
26. Keep RF, Smith DE. Choroid plexus transport: gene deletion studies. *Fluids Barriers CNS*. 2011;8:26.
27. Praetorius J, Nejsum LN, Nielsen S. A SCL4A10 gene product maps selectively to the basolateral plasma membrane of choroid plexus epithelial cells. *Am J Physiol Cell Physiol*. 2004;286:C601–C610.
28. Gunshin H, Allerson CR, Polycarpou-Schwarz M, Rofts A, Rogers JT, Kishi F, Hentze MW, Rouault TA, Andrews NC, Hediger MA. Iron-dependent regulation of the divalent metal ion transporter. *FEBS Lett*. 2001;509:309–316.
29. Lymboussaki A, Pignatti E, Montosi G, Garuti C, Haile DJ, Pietrangelo A. The role of the iron responsive element in the control of ferroportin1/IREG1/MTP1 gene expression. *J Hepatol*. 2003;39:710–715.